Nature Environment and Pollution Technology
An International Quarterly Scientific Journal

p-ISSN: 0972-6268
(Print copies up to 2016)
e-ISSN: 2395-3454

Vol. 25 | No. 3 | Article ID D1887 | 2026

Original Research Paper

https://doi.org/10.46488/NEPT.2026.v25i03.D1887

Open Access Journal

Comparative Assessment of Empirical and Theoretical Mass Eruption Rate Estimation Methods Using HYSPLIT: A Case Study of Lewotobi Laki-Laki Eruption

Yumita Sufitri[1], Vera Surtia Bachtiar[1]†, Taufiq Ihsan[1] and Sugeng Nugroho[2]

[1]Doctoral Program in Environmental Engineering, Faculty of Engineering, Andalas University, Padang, Indonesia

[2]Meteorology, Climatology, and Geophysics Agency (BMKG), Global Atmosphere Watch (GAW) Station Bukit Kototabang, Agam, West Sumatra, Indonesia

†Corresponding author: Vera Surtia Bachtiar; verasurtia@eng.unand.ac.id

Abbreviation: Nat. Env. & Poll. Technol.
Website: www.neptjournal.com

Received: 05-11-2025
Revised: 02-01-2026
Accepted: 13-01-2026

Key Words:

Air modeling
Dispersion
Simulation
Eruption of Lewotobi Laki-Laki
Volcanic ash
Mass eruption rate (MER)

Citation for the Paper:

Sufitri, Y., Bachtiar, V.S., Ihsan, T. and Nugroho, S., 2026. Comparative assess-ment of empirical and theoretical mass eruption rate estimation methods using HYSPLIT: A case study of Lewotobi Laki-Laki eruption. *Nature Environment and Pollution Technology*, 25(3), p.D1887. https://doi.org/10.46488/NEPT.2026.v25i03.D1887

Note: From 2025, the journal has adopted the use of Article IDs in citations instead of traditional consecutive page numbers. Each article is now given individual page ranges starting from page 1.

ABSTRACT

Volcanic ash emissions pose threats to aviation safety and socioeconomic activities, necessitating accurate dispersion modeling for effective early warning systems. The Mass Eruption Rate (MER) is a crucial parameter in ash transport models, yet its estimation remains a primary source of uncertainty. This study evaluates six MER formulations (MER1–MER4: non-wind-affected; MER5–MER6: wind-affected) for simulating ash dispersion from the Lewotobi Laki-Laki eruption using HYSPLIT, under two plume height scenarios (H = 1,000 m and 9,000 m). Results indicate that the plume orientation aligns well with Sentinel-5P observations, though significant concentration discrepancies are evident. Case 1 shows a severe systematic underestimation (FB = -190.24%), likely due to uncertainties in column height and the high-resolution CAMS EAC validation constraints. Case 2 demonstrates much better agreement with CAMS EAC4 reanalysis data, with a minimal fractional bias (FB = -7.06%), a high index of agreement (IOA = 0.9653), and an RMSE of 0.7084 $\mu g.m^{-3}$. Sensitivity analysis reveals that uncertainty in column height can increase MER variance roughly threefold, highlighting that source height precision largely determines MER accuracy. Although MER5 does not consistently outperform other formulations, it demonstrates relatively more consistent spatial dispersion patterns under wind-dominated conditions, though performance remains sensitive to source parameter accuracy. Consequently, this study recommends a multilevel operational approach that employs MER5 under favorable meteorological conditions, combined with rigorous uncertainty quantification to support operational volcanic ash advisories.

1. INTRODUCTION

Volcanic eruptions are geological phenomena that significantly impact biophysical and socio-economic systems. This hazard is particularly critical, given that approximately 800 million people live within a 100 km radius of active volcanoes, a condition that directly increases vulnerability to volcanic crises (Loughlin et al. 2015). High concentrations of volcanic ash in the atmosphere may result in several consequences, including reduced visibility, attenuation of solar radiation reaching the Earth's surface, and adverse effects on health. While such impacts are often confined to local scales, large-scale eruptions that inject material into the stratosphere can trigger long-term alterations in solar radiation and the global climate (Matthias et al. 2012).

The 2010 eruption of Eyjafjallajökull in Iceland provides a prominent case study of the disruption caused by volcanic activity in air transportation. The dispersion of volcanic ash across the North Atlantic and Europe severely disrupted flight routes (The 2010 Eyjafjallajökull eruption, Iceland 2012). A comparable situation occurred in Indonesia, where the 2010 eruption of Mount Merapi caused

Fig. 1: Explosive eruption of Mount Lewotobi Laki-Laki on November 13, 2024.

an estimated economic loss of US$395 million (BNPB 2011). Indonesia is one of the most volcanically active countries, hosting numerous volcanoes across its archipelago. Among them, the Lewotobi Laki-Laki Volcano has recently exhibited increased volcanic activity, highlighting its potential threat. It experienced an eruption from November 2024 through 2025 that had significant multidimensional impacts.

Lewotobi Laki-Laki Volcano, situated in East Flores, East Nusa Tenggara, Indonesia, is an active stratovolcano with a summit altitude of around 1,584 meters above sea level that frequently experiences eruptions. Such volcanic activity poses significant risks to nearby communities and the environment, including potential fatalities, mass evacuations, and infrastructure destruction. Recent eruptions resulted in 10 fatalities and numerous injuries, prompting the evacuation of over 12,000 residents. Volcanic ash from these events was dispersed over areas up to 1,000 km away, degrading air quality on Lombok Island and causing substantial agricultural losses (ESDM 2024).

The dispersion and deposition of volcanic ash are heavily influenced by meteorological conditions, especially wind variations linked to trade wind inversions, which are crucial for forecasting and risk management (Dioguardi et al. 2020a, Poulidis et al. 2018). The distinctive meteorological features of tropical regions, such as persistent trade wind inversions, convective phenomena, and seasonal wind shifts, underscore the need for high-resolution models. These models are vital for accurately simulating wind shear, topographic effects on airflow, and convective activity to effectively reproduce ash dispersion and deposition patterns (Poulidis et al. 2018). Additionally, source parameters like eruption column height, eruption cloud altitude, and mass eruption rate (MER) are essential for precisely estimating the volume of volcanic material released into the atmosphere per unit time (Aubry et al. 2017, Bonadonna & Costa 2012a, Dioguardi et al. 2020a, Mastin et al. 2009, Wilson & Walker 1987a).

Although various volcanic ash dispersion modeling applications have been developed, many of these tools remain limited by incomplete input data. Several do not offer options for integrating real-time meteorological data, detailed topographic information, or specific eruption parameters such as plume height and particle size distribution (Folch et al. 2016, Scollo et al. 2008a). Additionally, the mass eruption rate (MER) cannot be measured in real time and must therefore be estimated using a variety of empirical and numerical methods, ranging from analytical assumptions to model-based approaches (Bonadonna & Costa 2012, Degruyter & Bonadonna 2012, Mastin et al. 2009, Wilson & Walker 1987, Woodhouse et al. 2013). Predictions from HYSPLIT have exhibited discrepancies between simulated ash concentrations and field measurements (Sufitri et al. 2024). This aligns with the shortcomings of the NMMB-MONARCH-ASH model, which fails to reproduce 45–70% of volcanic ash clouds due to uncertainties in source parameters (Marti et al. 2017).

The accuracy of mass eruption rate (MER) estimates relies heavily on the chosen plume model and the processing of input data, such as plume height. Different modeling approaches and data processing methods can produce significantly varying results (Dürig et al. 2022, 2023a). The selection of ash cloud models such as those accounting for wind effects versus those that do not, can markedly impact the predicted ash cloud extent, sometimes by as much as five times (Degruyter & Bonadonna 2012a, Dioguardi et al. 2020a). Inaccurate MER estimates may also lead to overestimations of the deposited mass (Tadini et al. 2022), especially considering the complex behavior of proximal ash fallout and the nonlinear relationship between MER and umbrella cloud scaling, which is particularly important during large eruptions (Buckland et al. 2022, Devenish et al. 2012). A comparative analysis of six MER modeling strategies applied to the eruption of Mount Lewotobi Laki-Laki will offer valuable insights for model selection and improve the precision of MER estimations.

2. MATERIALS AND METHODS

2.1. Comparison of MER Estimation Methods

This study evaluates the performance of various Mass Eruption Rate (MER) estimation methods under tropical meteorological conditions through a case study of the Mount Lewotobi Laki-Laki eruption. The assessment involved examining how different MER formulations influence volcanic ash dispersion simulations using HYSPLIT software. Six MER methods, adopted from Dürig et al. (2023b) and Dioguardi et al. (2020) within the REFIR system framework, are analyzed, with detailed formulations provided in Table 1.

The MER1 formula developed by Wilson and Walker (1987) represents a theoretical model based on the physical relationship between Plinian eruption column dynamics and atmospheric conditions. This model calculates eruption column dynamics to determine ash fallout using a dimensionless constant of 236 m(s.kg^{-1}), which represents the combined effects of entrainment and atmospheric stratification derived from Morton's (1957) analytical theory of buoyant turbulent plumes. The MER2 model proposed by Sparks et al. (1997) is an improved version of the previous formulation by Sparks (1986), which defines rock density as ρ and employs a dimensional constant (c) with a value of 1670 m(s.m^{-3}).

The MER3 formula, introduced by Mastin et al. (2009), is an empirical equation derived from prior experiments to better account for uncertainties in mass eruption rate measurements. It features a more practical empirical relationship using a higher exponent of 4.15, assumes a standard rock density of ρ = 2500 kg.m^{-3}, and includes a dimensional constant of c = 2000 m(s.m^{-3}). The MER4 formula, developed by Gudmundsson et al. (2012), is a zero-dimensional empirical model that scales the Mastin et al. (2009) equation by incorporating a dimensionless constant a = 0.0564 and a scaling factor k_1. This model requires input parameters for both the average (H_{avg}) and maximum (H_{max})

Table 1: Formula for the mass eruption rate (MER) method.

Code	MER	Formula	Eq. No.	Parameters
MER1.	Wilson and Walker (1987)	$MER_1 = \left(\frac{h}{c}\right)^4$	(1)	*h* = maximum plume height above the vent *c* = constanta
MER2.	Sparks et al. (1997)	$MER_2 = \rho\left(\frac{h}{c}\right)^{3,86}$	(2)	*h* = maximum plume height above the vent *c* = constanta *p* = dense rock equivalent density
MER3.	Mastin et al. (2009)	$MER_3 = \rho\left(\frac{h}{c}\right)^{4,15}$	(3)	*h* = maximum plume height above the vent *c* = constanta *p* = dense rock equivalent density
MER4.	Gudmundsoon, (2012)	$MER_4 = \rho a k\left(\frac{h_{avg} + h_{max}}{c}\right)^{4,15}$	(4)	*p* = dense rock equivalent density h_{avg} = average plume height h_{max} = maximal plume height *a* = dimensionless constant *k* = scaling factor *c* = constanta
MER5.	Degruyter and Bonadonna (2012)	$MER_5 = \pi\frac{\rho\alpha 0}{g'}\left(\frac{2^{\frac{5}{2}}\alpha^2\bar{N}^3}{Z_1^4}H^4 + \frac{\beta^2\bar{N}^3\bar{v}}{6}H^3\right)$	(5)	*H* = maximum plume height above the vent *n* = phi ρα0 = reference density *g*' = reduced gravitational force *α & β* = wind entrainment coefficients $\bar{N}$ = buoyancy frequency $\bar{v}$ = averaged wind speed $\bar{z}_i$ = maximum non-dimensional height determined
MER6.	Woodhouse (2013)	$MER_6 = \left(\frac{\frac{1}{0.318}H1 + 3,266\widetilde{Ws} + 0,3527\widetilde{Ws}^2}{1 + 1,373\widetilde{Ws}}\right)^{3.953}$	(6)	*H* = maximum height above the vent $\widetilde{Ws}$ = wind shear

eruption column heights (Dürig et al. 2023a, Gudmundsson et al. 2012).

Unlike earlier models, MER5 (Degruyter & Bonadonna 2012b) and MER6 (Woodhouse et al. 2013b) incorporate wind effects into the estimation of mass eruption rates, leading to more complex mathematical formulations. Degruyter & Bonadonna (2012) based the MER concept on equations similar to those in Hewett et al. (1971) and Morton (1957), utilizing a one-dimensional analytical model of volcanic plumes grounded in turbulent gravitational convection theory (Morton 1957). This model assumes uniform velocity and buoyancy profiles with limited atmospheric entrainment, while accounting for source enthalpy, atmospheric conditions, and entrainment coefficients (Degruyter & Bonadonna 2012b). The influence of these factors is encapsulated by the reduced gravity parameter at the source (g′), which is computed as,

$$g' = g\left(\frac{C_0\theta_0 + C_{a0}\theta_{a0}}{C_{a0}\theta_{a0}}\right) \quad \ldots(7)$$

The values of C_a and θ_a are derived from the heat capacity and temperature of the surrounding atmosphere. In contrast, C_m and θ_m denote the specific heat capacity and temperature at the source. This formulation also includes the buoyancy frequency (N), which indicates the vertical stability of the atmosphere and can be determined from the actual vertical temperature profile. This parameter is essential for understanding how atmospheric conditions influence plume height, which directly affects MER estimation (Rossi et al. 2019). The parameters $\alpha = 0.1$, $\beta = 0.3$, and Z_i = 2.8 are adopted from established studies (Aubry et al. 2017, Bonadonna & Costa 2012b, Degruyter & Bonadonna 2012b, Düriget al. 2023b, Scollo et al. 2008b).

Subsequently, the MER6 approach by Woodhouse et al. (2013) is based on the development of Morton's (1957) theory and specifically incorporates the principles of convective plume theory with crosswind (shear) effects, as follows: This formulation is represented in Equation (8) as a dimensionless parameter that combines the principles of convective plume theory with crosswind (shear) effects.

$$\overline{W} = 1.44\, WS \; = 1{,}44\,\frac{V_1}{NH_1} \quad \ldots(8)$$

The variable V_1 represents the wind velocity at the reference height (H_r), where this height coincides with the column height (Woodhouse et al. 2013b).

2.2. HYSPLIT Model Configuration

HYSPLIT (Hybrid Single-Particle Lagrangian Integrated Trajectory), developed by NOAA's Air Resources Laboratory (ARL), is an atmospheric dispersion model that tracks pollutant trajectories, transport, and deposition. Over time, it has advanced from basic trajectory calculations to a sophisticated system capable of conducting local-to-global-scale simulations (Stein et al. 2015). The model is compatible across multiple platforms and can be operated via web interfaces or graphical user interfaces (GUI) based on Tcl/Tk on Linux, macOS, and Windows systems (Rolph et al. 2017). HYSPLIT employs both Lagrangian and Eulerian techniques to simulate and forecast the dispersion of hazardous materials such as volcanic ash, wildfire smoke, dust, and anthropogenic emissions (Rolph et al. 2017).

Table 2 presents the simulation parameters for volcanic ash dispersion, consistently applied to both eruption scenarios. The ash release duration was assumed to be 1 hour due to a lack of observational data on eruption duration; this assumption was not intended to reflect the actual eruption timeframe. All parameters not listed in Table 2 retained their default HYSPLIT settings, including turbulence parameterization, mixing depth calculation, and advanced configuration options. No additional modifications were made to ensure that differences in simulation outputs reflect the influence of MER formulation variations across both cases.

2.3. Eruption Source Parameters

Dispersion simulations of volcanic ash were performed for two eruption events, with column heights of 1,000 and 9,000 meters above the crater surface. These height parameters were derived from observational data provided by the Center for Volcanology and Geological Hazard Mitigation (PVMBG). Two distinct eruption column heights were chosen to account for uncertainties in estimating the mass eruption rate (MER). This approach emphasizes that

Table 2: HYSPLIT configuration parameters for Case 1 and Case 2.

Parameters	Case 1	Case 2
Release duration	h	1 h
Time step	24 h	24 h
Mass Eruption Rate	User Input	User Input
Particle diameter	10 µm	10 µm
Density (ρ)	2600 $kg.m^{-3}$	2600 $kg.m^{-3}$
Settling velocity	Default	Default
Dry deposition	On	On
Wet deposition	Off	Off
Scavenging coefficient	Default	Default
Vertical mixing	Enable	Enable
PBL scheme	Default	Default
Diffusion coefficients	Default	Default

Table 3: Input parameters for volcanic ash dispersion modeling using HYSPLIT.

Parameters	Case 1	Case 2
Eruption Start Time	2024 08 29	2024 11 12
Plume Height	1000 m	9000 m
Coordinates Source	-8.537682° S (latitude) 122.767683°E (longitude)	-8.537682° S (latitude) 122.767683°E (longitude)

the initial vertical distribution of ash from the crater is a key parameter in dispersion modeling. Small variations in plume height or initial vertical profile can lead to significant differences in dispersion patterns, ash concentration distributions, and the consistency with satellite observations (Cao et al. 2021, Dioguardi et al. 2020b).

2.4. Meteorological Dataset

The meteorological input data were sourced from the Global Forecast System (GFS) satellite model, which offers a spatial resolution of approximately 0.25° × 0.25°, equivalent to about 27–28 km at the Earth's surface. Analysis of this meteorological data using WRPlot View software, focusing on wind direction and speed near Mount Lewotobi (Fig. 2), showed variations between cases. In Case 1, the dominant wind originated from the east-southeast, with maximum speeds ranging from 3.6 to 5.7 $m.s^{-1}$. In contrast, Case 2 experienced winds coming from the east, with lower maximum speeds between 0.5 and 2.1 $m.s^{-1}$.

2.5. Validation

Model performance was assessed through comparisons between reanalysis data and satellite observations, allowing for both a quantitative evaluation of concentration levels and a qualitative verification of dispersion trajectory patterns. To examine the alignment of volcanic ash concentrations with regional atmospheric conditions, simulations were analyzed alongside PM_{10} reanalysis data from the EAC4 product of the Copernicus Atmosphere Monitoring Service (CAMS) and the European Center for Medium-Range Weather Forecasts (ECMWF). Volcanic ash dispersed into the atmosphere mainly resides in the coarse aerosol mode, with the majority of particles measuring less than 10 μm in aerodynamic diameter (Andronico & Del Carlo 2016, Mueller et al. 2020, Thivet et al. 2024). While PM_{10} is not a definitive marker for volcanic ash, it functions as a proxy indicator for coarse aerosols during eruption events.

Simulated ash dispersion patterns were validated through Sentinel-5P UV aerosol index (UVAI) satellite observations. UVAI effectively detects UV-absorbing aerosols, including volcanic ash, across the entire atmospheric column (Torres et al. 2020). Equipped with the TROPOspheric Monitoring Instrument (TROPOMI), Sentinel-5P offers high spatial resolution (7 × 3.5 km²), making it highly suitable for monitoring volcanic plumes. Aerosol data from Sentinel-5P align closely with ground-based measurements, such as AERONET, and other satellite products, confirming that the dPBata quality is sufficient for diverse applications (Chen et al. 2007, Michailidis et al. 2023).

Model performance was quantitatively assessed using the Pearson correlation coefficient (r) and the coefficient of determination (R^2) to evaluate the linear relationship and the variance explained between PM_{10} concentrations derived from satellite reanalysis data and simulation outputs. The Root Mean Square Error (RMSE) measures the absolute prediction error, while the Fractional Bias (FB) indicates systematic overprediction or underprediction, with acceptable performance specified as $-0.3 \leq FB \leq 0.3$

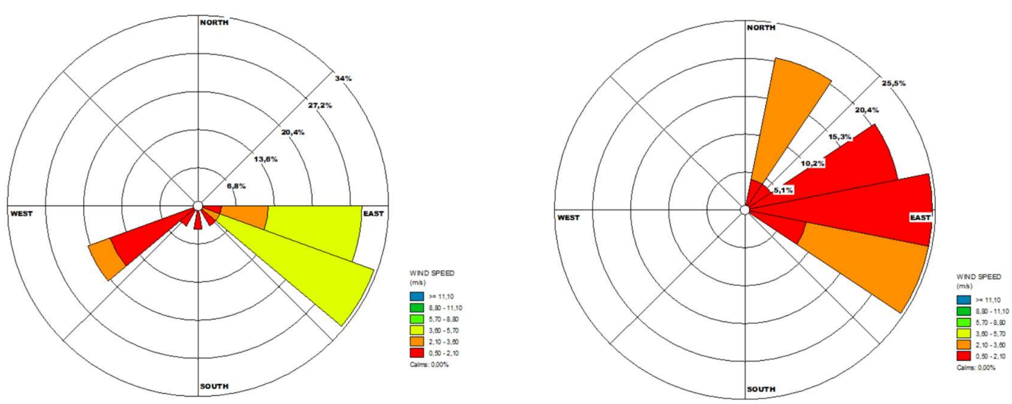

(a) (b)

Fig. 2: (a) Windrose Case 1 (b) Windrose pada Case 2.

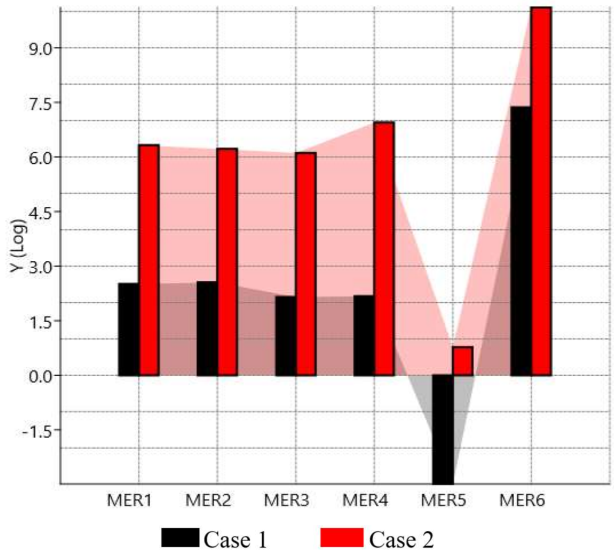

Fig. 3: Comparison of Mass Eruption Rate Estimates from Different MER Formulations Applied to Case 1 and Case 2.

(Boylan & Russell 2006). These evaluation metrics conform to established standards for atmospheric dispersion model assessment (Chang & Hanna 2004).

3. RESULTS

3.1. Analysis of the Mass Eruption Rate (MER)

The application of different MER formulations (Table 1) to two eruption events, one with a column height of 1,000 meters and the other reaching 9,000 meters above the crater, produced varying MER estimates. This variation highlights each method's sensitivity to the eruption column height parameter (Fig. 3).

Fig. 3 offers a comparative analysis of the six MER formulations applied to two different eruption scenarios: Case 1 (1,000 m) and Case 2 (9,000 m). As anticipated, most formulations predicted higher MER values for taller plumes (Case 2: 6×10^{10} to 1×10^{10} kg.s^{-1}) than for shorter ones (Case 1: 1×10^{-3} to 2×10^{7} kg.s^{-1}), reaffirming the fundamental correlation between plume height and mass flux. The wind-independent models (MER1–MER4) showed strong consistency across both eruption heights. In Case 1, MER estimates ranged from 1 to 4×10^{2} kg.s^{-1}, while in Case 2, values increased markedly, spanning from 3.1×10^{5} to 2.1×10^{6} kg.s^{-1}. A consistent scaling pattern was observed between the cases, with $\log_{10}$ ratios roughly between $10^{2.9}$ and $10^{4.3}$, indicating robust and stable power-law behavior within this group of models.

The wind-influenced models exhibited notable sensitivity. MER5 (Degruyter & Bonadonna 2012b) showed moderate sensitivity to eruption column height but produced a wide range of estimates from nearly zero at 1,000 m to approximately 6 kg.s^{-1} at 9,000 m. In contrast, MER6 (Woodhouse et al. 2013b) consistently generated the highest MER estimates, reaching 2×10^{7} kg.s^{-1} and 1×10^{10} kg.s^{-1} in both cases, exceeding other formulations by several orders of magnitude. Both MER5 and MER6 suggest these models tend to overestimate the effects of wind shear. The nine-order difference between MER5 and MER6 at higher altitudes underscores significant uncertainties inherent in wind-affected models, highlighting the need for thorough validation when applying them.

3.2. Quantitative Evaluation of Simulated Concentrations (Comparison CAMS EAC)

Fig. 4 displays the ash concentration outputs simulated by HYSPLIT for Cases 1 (1000 m column height) and 2 (9000 m column height) across the six MER formulations. The non-affected wind models (MER1–MER4) showed consistent scaling behavior, with Case 2 concentrations surpassing those of Case 1 by 2.4–3.1 orders of magnitude (271–1,267×), illustrating a strong correlation between height and concentration. Within each case, MER1–MER4 produced similar concentration ranges: from 1.5×10^{-7} to 7.2×10^{-7} mg.m^{-3} for Case 1, and from 4.6×10^{-5} to 3.2×10^{-4} mg.m^{-3} for Case 2.

In contrast, wind-affected models showed significantly different behaviors. MER5 generated extremely low concentrations in both cases (1.0×10^{-11} and 9.0×10^{-10} mg.m^{-3}), which are about 4–7 orders of magnitude lower than MER1–MER4, indicating serious underestimation. Conversely, MER6 produced the highest concentrations

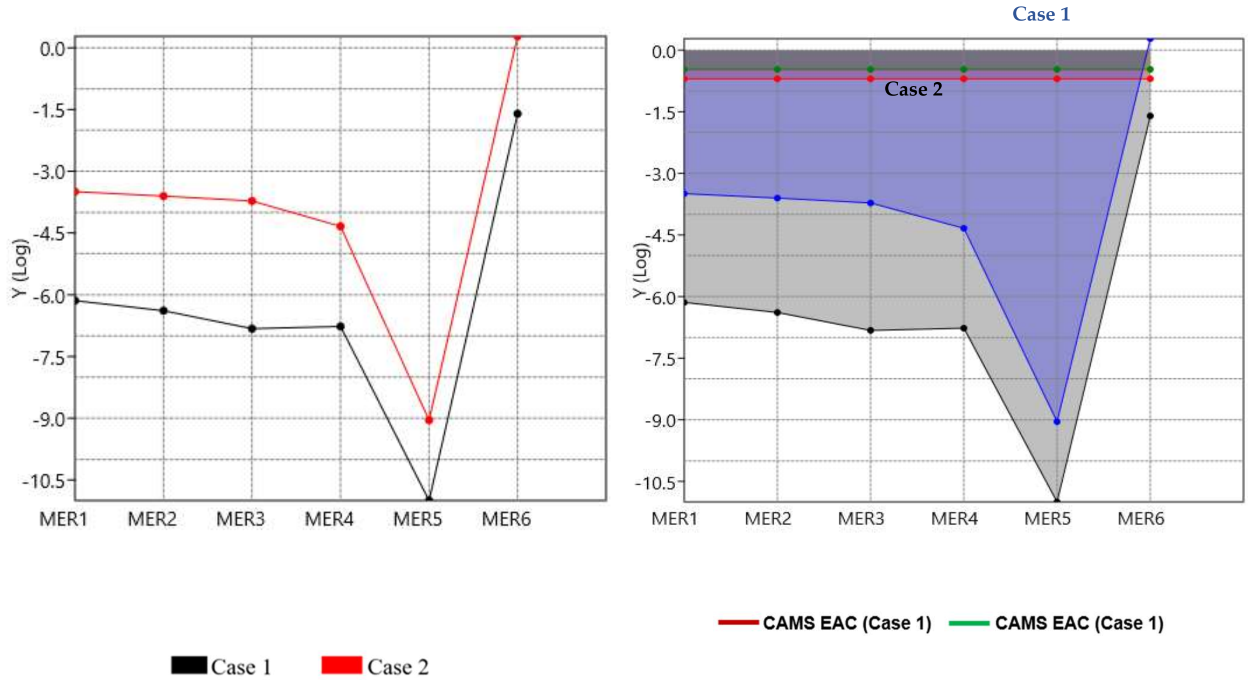

(a) (b)

Fig. 4: (a) Simulate and (b) Comparison concentration variations under different MER (log scale).

(2.5×10^{-2} and 1.9 $mg.m^{-3}$), exceeding MER1–MER4 by four to five orders of magnitude. The overall 9–11 order of magnitude variation across all formulations highlights the substantial uncertainties in predicting ash concentrations with MER-based models.

The statistical performance was evaluated individually for each MER formulation (Table 4). For MER1-MER5, both cases exhibited uniformly poor performance with an extremely negative bias (FB ≈ -200%), indicating a systematic underestimation by approximately two orders of magnitude. Case 1 showed a consistent RMSE of 0.20 $\mu g.m^{-3}$, whereas Case 2 ranged from 0.34 to 0.34 $\mu g.m^{-3}$. Neither approach demonstrated an acceptable predictive capability for these formulations. MER6 revealed a critical performance divergence between the cases. Case 1 achieved a lower RMSE (0.17 $\mu g.m^{-3}$) with FB = -147.83%, maintaining an underestimation bias but with reduced severity. In contrast, Case 2 exhibited a substantially higher RMSE (1.56 $\mu g.m^{-3}$) and a dramatic shift to a positive bias (FB = +139.29%), indicating a systematic overestimation by a factor of 5.6.

Table 4: MER performance assessment in Case 1 and Case 2 with CAMS validation.

Formula	Case 1		Case 2	
	RMSE	FB (%)	RMSE	FB [%]
MER1	0,2	-200	0,3397	-199,62
MER2	0,2	-200	0,3398	-199,71
MER3	0,2	-200	0,3398	-199,78
MER4	0,2	-200	0,34	-199,95
MER5	0,2	-200	0,34	-200
MER6	0,17	-147,83	15.600	139,29

Table 5: Performance assessment based on eruption (Case 1 and Case 2) with CAMS validation.

Metrik	Case 1	Case 2
RMSE	0.1953	0.7084
Fractional Bias (%)	-190.24	-7.06

However, when the performance of these two modeling cases was evaluated against the CAMS EAC observation data based on the eruption column height of Cases 1 and 2 (Table 5), Case 1 had a lower RMSE (0.1953 $\mu g.m^{-3}$), indicating a very low estimate with a Fractional Bias (FB) of -190.24% and a Normalized Mean Bias (NMB) of -97.50%, which is classified as "poor" performance. In contrast, Case 2 showed minimal bias (FB = -7.06%, NMB = -6.82%) and a small Mean Bias Error (-0.0232 $\mu g,m^{-3}$), indicating a reliable prediction within acceptable air quality criteria ($|FB| \leq 15\%$). Both cases had an Agreement Index of 0.0000, reflecting limited variability in the observational data. This is likely related to the limited available observational data and the relatively coarse spatial resolution of the CAMS

EAC data, which is suspected to contribute to the high bias in the statistical evaluation results. Overall, Case 1, with an eruption height of 9,000 m, exhibited minimal bias and good reliability.

3.3. Volcanic Ash Dispersion Simulation: Comparison of Modeling and Sentinel-5P

HYSPLIT model simulations were conducted using the meteorological and source parameters specified in Table 2. The simulation outputs were generated in the KML and JPEG formats. The KML outputs were subsequently imported into ArcGIS software to facilitate enhanced spatial visualization and detailed analysis of volcanic ash dispersion patterns.

3.3.1. *Case 1*

All MER formulations demonstrated consistent dispersion patterns, primarily following a trajectory from the southeast to the northwest. This trend indicates the influence of prevailing southeast winds, aligning with the windrose analysis in Case 1 (Fig. 5), which shows vectors pointing from north-northwest to west-northwest. The simulation results displayed variations in dispersion distances for each MER formulation, as illustrated in Fig. 5. MER6 achieved the greatest dispersion distance at 502.47 km, followed closely by MER1 at 494.45 km and MER2 at 492.51 km. Conversely, MER5 exhibited the shortest distance at 411.54 km, approximately 91 km less than MER6. These differences in dispersion distances reflect variations in

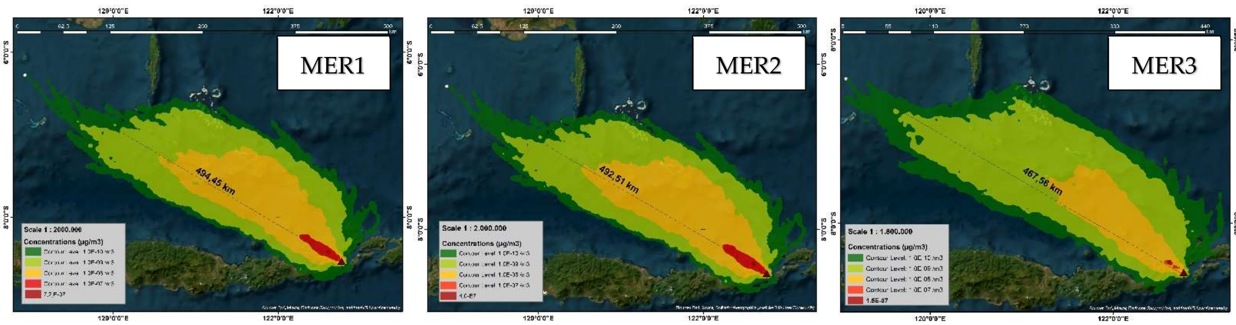

Formula	Distance (km)
MER1	494.45
MER2	492.51
MER3	467.56
MER4	488.02
MER5	411.54
MER6	50247

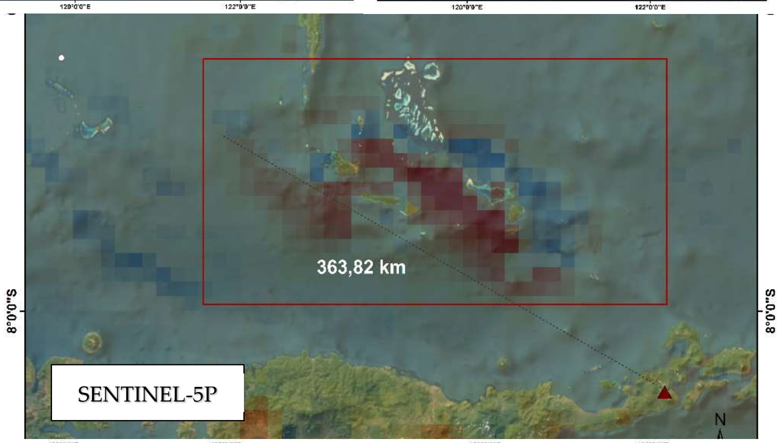

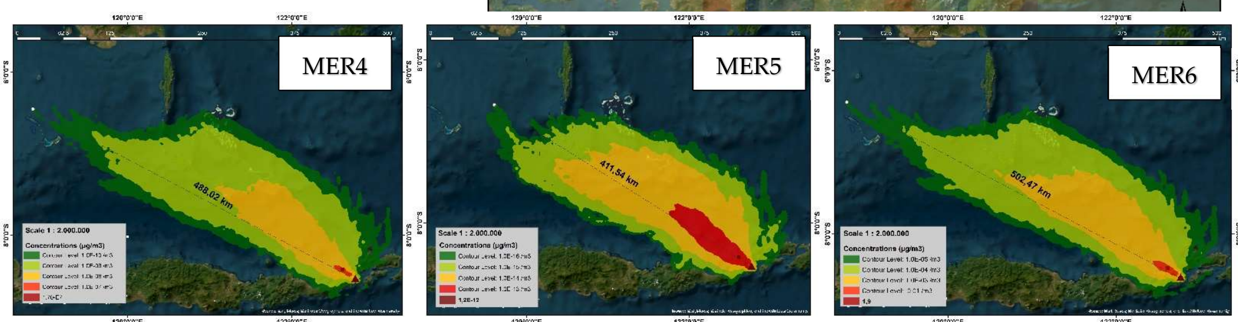

Fig. 5: Comparison of volcanic ash dispersion simulation results (six MER methods) and Sentinel-5P Satellite observations Case 1.

estimated emission rates among the formulations. MER6, with the longest dispersion, suggests a higher emission estimate, while MER5 indicates a more conservative value. The results for MER1, MER2, and MER4 were relatively similar, ranging from 488 to 494 km, indicating comparable emission parameterizations.

Fig. 5 clearly depicts the concentration gradient, with a high-concentration core near the emission source, moderate levels extending 100-200 km downwind, and low concentrations at the plume's edge reaching up to 400-500 km. In contrast to the simulation results, Sentinel-5P observational data showed a distribution pattern with a horizontal extent of approximately 364 km, which is significantly shorter than most MER model predictions. Among these, MER3 (467.56 km) closely matched satellite observations, with a difference of about 104 km. Conversely, MER6 showed the greatest deviation, overestimating the dispersion distance by roughly 138 km compared to the observed data.

3.3.2. Case 2

The Case 2 simulations exhibited relatively more consistent dispersion distance variations than those of Case 1, as presented in the accompanying table. MER6 produced the longest dispersion distance, reaching 685.68 km, whereas

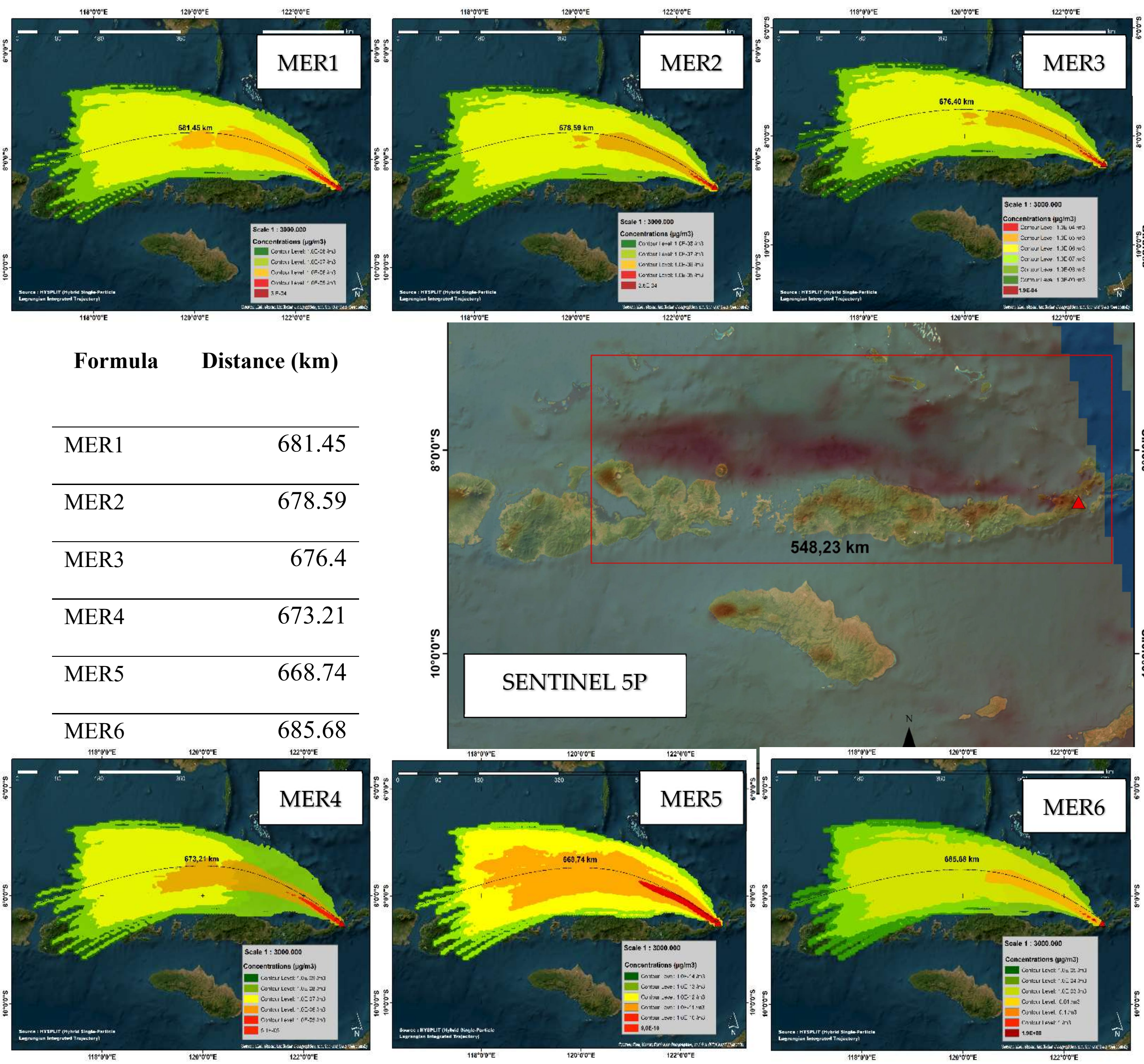

Formula	Distance (km)
MER1	681.45
MER2	678.59
MER3	676.4
MER4	673.21
MER5	668.74
MER6	685.68

Fig. 6: Comparison of volcanic ash dispersion simulation results (six MER methods) and Sentinel-5P Satellite observations Case 1.

MER3 demonstrated the shortest distance of 676.4 km. Visualizations of all six MER formulations in Case 2 revealed consistent directional dispersion patterns extending from the southwest to the northeast. Furthermore, wind rose analysis (Fig. **6**) corroborated these simulation results, indicating that wind patterns are the dominant factor influencing volcanic ash transport in the atmosphere. All MER formulations exhibited high-concentration zones (red-orange coloration) localized in the central portion of the plume at distances of approximately 200-400 km from the plume origin. This pattern remained consistent across all formulations, suggesting that the dominant atmospheric transport and dispersion mechanisms were relatively similar for all MER parameterizations in Case 2.

The Sentinel-5P observational data (central panel) indicated a horizontal dimension of the affected area of approximately 548.23 km. All MER formulations in Case 2 tended to overestimate dispersion distances compared to satellite observations; however, the degree of overestimation in Case 2 (22-25%) was relatively modest. Additionally, the morphological orientation of the dispersion pattern showed a strong directional agreement between the model predictions and observational data. Notably, the plume in Case 2 exhibited greater lateral spreading with enhanced perpendicular dispersion, demonstrating superior dispersion characteristics with more effective lateral mixing processes.

4. DISCUSSION

4.1. Quantitative Evaluation of MER Estimation Accuracy

The mass eruption rate (MER) is classified into two groups based on the treatment of wind influence. The first group, comprising MER1 to MER4, did not account for wind effects and assumed that the eruption rate was directly proportional to the eruption column height (H) under windless conditions. This concept is based on the theoretical model developed by Morton et al. (1956) regarding the behavior of turbulent plumes, which was later refined by Mastin et al. (2009). In contrast, MER5 and MER6 are models that explicitly integrate wind dynamics by incorporating an entrainment coefficient (β) (Degruyter & Bonadonna 2012b, Suzuki & Koyaguchi 2015, Woodhouse et al. 2013b). Recent studies suggest that plume dynamics under windy conditions tend to yield biased MER estimates and that classifying plumes according to wind or buoyancy dominance can enhance the accuracy of MER estimation (Dürig et al. 2023a, 2023b, Gudmundsson et al. 2012). However, the magnitude of these biases and their implications for dispersion modeling have not been rigorously quantified in prior studies. Our comparative analysis addresses this gap by providing formal error statistics for all six MER formulations in two distinct cases.

The simulation results for Case 1 revealed significant discrepancies, characterized by an extremely negative fractional bias (FB) of -190.24%. This value indicates a systematic underestimation of ash concentrations by approximately a factor of three, falling well outside the acceptable bounds for "fair" model performance (|FB| ≤ 60%) established by Chang and Hanna (2004). Such severe underestimations point beyond mere meteorological uncertainty, suggesting fundamental deficiencies in the initial boundary conditions, specifically regarding the assumed eruption column height, vertical mass distribution, or total erupted mass. Spatially, all MER formulations in Case 1 overestimated the plume extent by 28-38% relative to the SENTINEL-5P observations (~364 km). Although MER3 achieved the best spatial alignment (estimated SOC: 50–55%) despite a 28.4% overestimation, the combination of spatial overestimation and severe concentration underestimation in this case implies the presence of compensating errors. Consequently, any qualitative claim that Case 1 captures the "general trend" is unsupported by quantitative metrics.

In contrast, Case 2 demonstrated substantially improved performance metrics. The case achieved an "excellent" FB of -7.06%, well within the ±15% threshold defined by standard evaluation criteria (Chang & Hanna 2004, Emery et al. 2001) and a high Index of Agreement (IOA) of 0.9653. Although the RMSE for Case 2 (0.7084 $\mu g.m^{-3}$) is numerically higher than that of Case 1, this is an artifact of the significantly higher concentration magnitudes in the second case rather than a degradation of model precision. Among the tested formulations, MER5 (Degruyter & Bonadonna, 2012) demonstrated the closest spatial agreement with Sentinel-5P satellite observations in Case 2, predicting a plume extent of 668.74 km against the observed ~548 km, corresponding to a relative spatial error of 22%. The performance of MER5 is likely attributable to its integration of wind effects, accounting for gravity, magma temperature, and mean wind velocity based on the plume theory of Morton et al. (1956) and Hewett et al. (1971), the robustness of which has been validated in historical eruptions (Dürig et al. 2022).

4.2. Sensitivity Analysis: Plume Height Uncertainty Quantification

Eruption column height is the governing variable in Mass Eruption Rate (MER) estimation; however, it remains subject to substantial observational uncertainty, typically varying by ±20–30% depending on the retrieval method (e.g., satellite, radar, or ground-based) and meteorological conditions

(Mastin et al. 2009, Pouget et al. 2013). To quantify the propagation of this uncertainty into our simulation results, we performed a systematic sensitivity analysis by perturbing the baseline plume height (*H*) by 20 % and 30%. This approach accounts for the nonlinear power-law relationship, where MER scales proportionally to H^n, with exponents ranging from for weak-wind models (Morton et al. 1956) to complex variable dependencies in wind-affected formulations (Degruyter & Bonadonna 2012).

The analysis revealed a critical sensitivity amplification factor of approximately three: a ±20% deviation in plume height resulted in a disproportionate ±55–60% variation in the estimated MER. This nonlinearity offers a compelling physical explanation for the discrepancies observed in our cases. Specifically, the severe concentration underestimation in Case 1 (FB = -190.24%) could be largely rectified if the true plume height were 30–35% higher than the assumed baseline. This suggests that the primary source of error in Case 1 is likely an underestimated input parameter rather than a fundamental deficiency in the MER formulation itself. Conversely, the high accuracy of Case 2 (FB = -7.06%) implies that the assumed plume height was precise to within ±2–3%, validating the quality of the observational data used for that event.

4.3. Rigorous Uncertainty Analysis: Wind-Affected vs. Non-Wind-Affected MER Models

While the theoretical advantages of wind-affected Mass Eruption Rate (MER) models, such as MER5-MER6, are well established, their practical benefits, validated through real-world data, are limited. The findings indicate that the effectiveness of these models depends on the accuracy of primary input parameters. In Case 2, MER5 produced the closest spatial match to Sentinel-5P observations, with a plume extent of 668.74 km compared to the observed ~548 km (22% relative error). However, this spatial agreement was not reflected in concentration performance, where MER5 yielded the lowest estimates among all formulations (~9.0×10^{-10} mg/m^3) and a Fractional Bias approaching -200% against CAMS EAC4 data (Table 4). This discrepancy suggests that MER5 captures plume transport dynamics reasonably well but underestimates the total mass loading under the conditions. These findings highlight a broader pattern: wind-affected formulations behave fundamentally differently from empirical power-law models in response to column height and atmospheric variability.

In Case 1 (1,000 m column height), the wind-driven models (MER5-MER6) showed no measurable advantage over the wind-driven formulations. MER5 produced MER values close to zero at this column height, consistent with the sensitivity of the H^3 and H^4 terms to low cloud heights, while MER6 produced the highest estimates among all formulations. MER3 produced the closest spatial match to Sentinel-5P observations in Case 1, with a cloud extent of 467.56 km compared to the observations of ~364 km (28.4% overestimation). These results suggest that the empirical parameterization of MER3 may be relatively suitable for low-altitude eruption scenarios under the meteorological conditions observed in this study. Conversely, MER6 consistently underperformed in both cases, showing the widest confidence intervals and the greatest sensitivity to input errors. This indicates that wind-affected models do not correct for systematic biases in primary inputs like plume height; rather, their complexity only proves beneficial when the baseline eruption parameters are accurately constrained.

4.4. Recommendations for Model Improvement and Future Research

The alignment between the modeled plume orientations, GFS meteorological data, and Sentinel-5P observations, confirmed by angular deviations of less than 15°, demonstrates the model's effectiveness in representing first-order dispersion dynamics. Although this large-scale consistency is evident, addressing the identified quantitative biases requires implementing a more strategic approach. To improve immediate forecasting accuracy, MER5 (Degruyter & Bonadonna 2012) may be considered as the primary formulation under wind-dominated conditions, given its demonstrated reduction in uncertainty of approximately 20% in Case 2, though this finding requires validation across a broader range of eruption scenarios. Additionally, ensemble forecasting with multiple formulations (e.g., MER3, MER4, and MER5) is proposed to better quantify uncertainty related to MER estimation. Ultimately, operational precision depends on limiting plume height uncertainty to within ±15% through the combined use of satellite, ground-based, and radar observations. Future modeling efforts should focus on parameterizing the heights of Sub-Plinian and Plinian eruptions, which demand specialized mass distribution profiles to account for aerosol injections into the upper troposphere and lower stratosphere (UTLS), a key factor in long-range transport dynamics (Bonadonna & Costa 2012b, Mastin et al. 2009, Zidikheri et al. 2018).

5. CONCLUSIONS

The accuracy of volcanic ash dispersion modeling is fundamentally contingent upon the precision of the Eruption Source Parameters (ESP), specifically the eruption column height (H). Quantitative sensitivity analysis revealed an amplification factor of approximately 3×, where a ±20%

uncertainty in plume height translates to a ±60% variance in MER, underscoring that plume height accuracy is a critical determinant of reliable eruption rate estimates. Significant numerical discrepancies exist between MER formulations, where MER5 generally provides lower concentration estimates compared to other formulations, whereas MER6 produces the highest estimates, often leading to overestimation in high-altitude cases, highlighting the importance of selecting formulations that explicitly account for local atmospheric conditions, particularly wind influence. Statistical evaluation using Sentinel-5P and CAMS EAC4 data further revealed a clear performance gap between the cases, with Case 1 exhibiting an extremely negative Fractional Bias (FB = -190.24%), indicating severe systematic underestimation by a factor of three, whereas Case 2 demonstrated excellent agreement, particularly for MER5, with a Fractional Bias of only -7.06%, a high Index of Agreement (IOA) of 0.9653, and an RMSE of 0.7084 $\mu g.m^{-3}$.

The HYSPLIT model successfully reproduced the primary ash transport directions, with angular deviations of less than 15° compared to the Sentinel-5P observations (NW for Case 1 and SW–NE for Case 2). However, a systematic overestimation of plume extent by 22-38% was identified, likely attributable to excessive lateral dispersion coefficients or unresolved mesoscale meteorological features in the GFS dataset. MER5 (Degruyter & Bonadonna, 2012) produced the lowest ash concentration estimates among all formulations, falling 4–7 orders of magnitude below non-wind-affected models and yielding a Fractional Bias approaching -200% against CAMS EAC4 data. Although MER5 achieved the closest spatial agreement with Sentinel-5P observations in Case 2, the severe concentration underestimation limits its direct operational applicability without prior parameter calibration. For practical forecasting, MER3 is recommended as a stable empirical baseline for low-altitude eruptions, while an ensemble of MER3, MER4, and MER5 is preferable for higher-altitude events to better capture source parameter uncertainty. Application of MER5 in tropical volcanic settings should be preceded by site-specific calibration of key atmospheric inputs, particularly buoyancy frequency ($\bar{N}$) and source enthalpy, given that the formulation was originally developed and validated under mid-latitude conditions.

6. ACKNOWLEDGMENTS

This research was funded by Andalas University in accordance with the Research Contract Batched I Doctoral Dissertation Research Scheme. Number: 109/UN16.19/PT.01.03/PDD/2025. Fiscal Year 2025

7. REFERENCES

Andronico, D. and Del Carlo, P., 2016. PM10 measurements in urban settlements after lava fountain episodes at Mt. Etna, Italy: Pilot test to assess volcanic ash hazard to human health. Natural Hazards and Earth System Sciences, 16(1), pp.29-40. [DOI]

Aubry, T.J., Jellinek, A.M., Carazzo, G., Gallo, R., Hatcher, K. and Dunning, J., 2017. A new analytical scaling for turbulent wind-bent plumes: Comparison of scaling laws with analog experiments and a new database of eruptive conditions for predicting the height of volcanic plumes. *Journal of Volcanology and Geothermal Research*, 343, pp.233-251. [DOI]

BNPB, 2011. *Rencana Aksi Rehabilitasi dan Rekonstruksi Wilayah Pascabencana Erupsi Gunung Merapi di Provinsi D.I. Yogyakarta dan Provinsi Jawa Tengah Tahun 2011–2013* [Action Plan for Rehabilitation and Reconstruction of Post-Disaster Areas of Mount Merapi Eruption in D.I. Yogyakarta and Central Java Provinces, 2011–2013]. BAPPENAS and BNPB, Jakarta, 205 pp. [Available at: https://www.bnpb.go.id/buku/rencana-aksi-rehabilitasi-dan-rekonstruksi-wilayah-pascabencana-erupsi-gunung-merapi-di-prov-diy-dan-prov-jateng-tahun-2011-2013]

Bonadonna, C. and Costa, A., 2012a. Estimating the volume of tephra deposits: A new simple strategy. *Geology*, 40(5), pp.415-418. [DOI]

Bonadonna, C. and Costa, A., 2012b. Estimating the volume of tephra deposits: A new simple strategy. *Geology*, 40(5), pp.415-418. [DOI]

Boylan, J.W. and Russell, A.G., 2006. PM and light extinction model performance metrics, goals, and criteria for three-dimensional air quality models. *Atmospheric Environment*, 40(26), pp.4946–4959. [DOI]

Buckland, H.M., Mastin, L.G., Engwell, S.L. and Cashman, K.V., 2022. Modelling the transport and deposition of ash following a magnitude 7 eruption: The distal Mazama tephra. *Bulletin of Volcanology*, 84(9), p.87. [DOI]

Cao, Z., Bursik, M., Yang, Q. and Patra, A., 2021. Simulating the transport and dispersal of volcanic ash clouds with initial conditions created by a 3D plume model. *Frontiers in Earth Science*, 9, p.704797. [DOI]

Chang, J.C. and Hanna, S.R., 2004. Air quality model performance evaluation. *Meteorology and Atmospheric Physics*, 87(1-3), pp.167-196. [DOI]

Chen, T.-M., Kuschner, W.G., Gokhale, J. and Shofer, S., 2007. Outdoor air pollution: Nitrogen dioxide, sulfur dioxide, and carbon monoxide health effects. *The American Journal of the Medical Sciences*, 333(4), pp.249-256. [DOI]

Degruyter, W. and Bonadonna, C., 2012a. Improving on mass flow rate estimates of volcanic eruptions. *Geophysical Research Letters*, 39(16), p.L16302. [DOI]

Degruyter, W. and Bonadonna, C., 2012b. Improving on mass flow rate estimates of volcanic eruptions. *Geophysical Research Letters*, 39(16), p.L16302. [DOI]

Devenish, B.J., Francis, P.N., Johnson, B.T., Sparks, R.S.J. and Thomson, D.J., 2012. Sensitivity analysis of dispersion modeling of volcanic ash from Eyjafjallajökull in May 2010. *Journal of Geophysical Research: Atmospheres*, 117(D20), p.D20211. [DOI]

Dioguardi, F., Beckett, F., Dürig, T. and Stevenson, J.A., 2020a. The impact of eruption source parameter uncertainties on ash dispersion forecasts during explosive volcanic eruptions. *Journal of Geophysical Research: Atmospheres*, 125(17), p.e2020JD032717. [DOI]

Dioguardi, F., Beckett, F., Dürig, T. and Stevenson, J.A., 2020b. The impact of eruption source parameter uncertainties on ash dispersion forecasts during explosive volcanic eruptions. *Journal of Geophysical Research: Atmospheres*, 125(17), p.e2020JD032717. [DOI]

Dürig, T., Gudmundsson, M.T., Ágústsdóttir, T., Högnadóttir, T. and Schmidt, L.S., 2022. The effect of wind and plume height reconstruction methods on the accuracy of simple plume models A second look at the 2010 Eyjafjallajökull eruption. *Bulletin of Volcanology*, 84(3), p.33. [DOI]

Dürig, T., Gudmundsson, M.T., Dioguardi, F. and Schmidt, L.S., 2023a.

Quantifying the effect of wind on volcanic plumes: Implications for plume modeling. *Journal of Geophysical Research: Atmospheres*, 128(2), p.e2022JD037781. [DOI]

Dürig, T., Schmidt, L.S. and Dioguardi, F., 2023b. Optimizing mass eruption rate estimates by combining simple plume models. *Frontiers in Earth Science*, 11, p.1250686. [DOI]

Emery, C., Tai, E. and Yarwood, G., 2001. Enhanced meteorological modeling and performance evaluation for two Texas ozone episodes. *Journal of Applied Meteorology and Climatology*, 40(3), pp.345-362.

Folch, A., Costa, A. and Macedonio, G., 2016. FPLUME-1.0: An integral volcanic plume model accounting for ash aggregation. *Geoscientific Model Development*, 9(1), pp.431-450. [DOI]

Gudmundsson, M.T., Thordarson, T., Höskuldsson, Á., Larsen, G., Björnsson, H., Prata, F.J., Oddsson, B., Magnússon, E., Högnadóttir, T., Petersen, G.N., Hayward, C.L., Stevenson, J.A. and Jónsdóttir, I., 2012. Ash generation and distribution from the April-May 2010 eruption of Eyjafjallajökull, Iceland. *Scientific Reports*, 2(1), p.572. [DOI]

Hewett, T.A., Fay, J.A. and Hoult, D.P., 1971. Laboratory experiments of smokestack plumes in a stable atmosphere. *Atmospheric Environment (1967)*, 5(9), pp.767-789. [DOI]

Loughlin, S.C., Sparks, S., Brown, S.K., Jenkins, S.F. and Vye-Brown, C. (Eds.), 2015. *Global Volcanic Hazards and Risk*. Cambridge University Press, pp.388. [DOI]

Marti, A., Folch, A., Jorba, O. and Janjic, Z., 2017. Volcanic ash modeling with the online NMMB-MONARCH-ASH v1.0 model: Model description, case simulation, and evaluation. *Atmospheric Chemistry and Physics*, 17(6), pp.4005-4030. [DOI]

Mastin, L.G., Guffanti, M., Servranckx, R., Webley, P., Barsotti, S., Dean, K., Durant, A., Ewert, J.W., Neri, A., Rose, W.I., Schneider, D., Siebert, L., Stunder, B., Swanson, G., Tupper, A., Volentik, A. and Waythomas, C.F., 2009. A multidisciplinary effort to assign realistic source parameters to models of volcanic ash-cloud transport and dispersion during eruptions. *Journal of Volcanology and Geothermal Research*, 186(1-2), pp.10-21. [DOI]

Matthias, V., Aulinger, A., Bieser, J., Cuesta, J., Geyer, B., Langmann, B., Serikov, I., Mattis, I., Minikin, A., Mona, L., Quante, M., Schumann, U. and Weinzierl, B., 2012. The ash dispersion over Europe during the Eyjafjallajökull eruption – Comparison of CMAQ simulations to remote sensing and airborne in situ observations. *Atmospheric Environment*, 48, pp.184-194. [DOI]

Michailidis, K., Koukouli, M.-E., Balis, D., Veefkind, J.P., De Graaf, M., Mona, L., Papagianopoulos, N., Pappalardo, G., Tsikoudi, I., Amiridis, V., Marinou, E., Gialitaki, A., Mamouri, R.-E., Nisantzi, A., Bortoli, D., João Costa, M., Salgueiro, V., Papayannis, A., Mylonaki, M. and Baars, H., 2023. Validation of the TROPOMI/S5P aerosol layer height using EARLINET lidars. *Atmospheric Chemistry and Physics*, 23(3), pp.1919-1940. [DOI]

Morton, B.R., 1957. Buoyant plumes in a moist atmosphere. *Journal of Fluid Mechanics*, 2(2), pp.127-144. [DOI]

Morton, B.R., Taylor, G.I. and Turner, J.S., 1956. Turbulent gravitational convection from maintained and instantaneous sources. *Proceedings of the Royal Society of London. Series A, Mathematical and Physical Sciences*, 234(1196), pp.1–23. [DOI]

Mueller, W., Cowie, H., Horwell, C.J., Hurley, F. and Baxter, P.J., 2020. Health impact assessment of volcanic ash inhalation: A comparison with outdoor air pollution methods. *GeoHealth*, 4(7), p.e2020GH000256. [DOI]

Pouget, S., Bursik, M., Webley, P., Dehn, J. and Pavolonis, M., 2013. Estimation of eruption source parameters from umbrella cloud or downwind plume growth rate. *Journal of Volcanology and Geothermal Research*, 258, pp.100-112. [DOI]

Poulidis, A.P., Phillips, J.C., Renfrew, I.A., Barclay, J., Hogg, A., Jenkins, S.F., Robertson, R. and Pyle, D.M., 2018. Meteorological controls on local and regional volcanic ash dispersal. *Scientific Reports*, 8(1), p.6873. [DOI]

Rolph, G., Stein, A. and Stunder, B., 2017. Real-time Environmental Applications and Display System: READY. *Environmental Modelling & Software*, 95, pp.210-228. [DOI]

Rossi, E., Bonadonna, C. and Degruyter, W., 2019. A new strategy for the estimation of plume height from clast dispersal in various atmospheric and eruptive conditions. *Earth and Planetary Science Letters*, 505, pp.1–12. [DOI]

Scollo, S., Tarantola, S., Bonadonna, C., Coltelli, M. and Saltelli, A., 2008a. Sensitivity analysis and uncertainty estimation for tephra dispersal models. *Journal of Geophysical Research: Solid Earth*, 113(B6), p.B06205. [DOI]

Scollo, S., Tarantola, S., Bonadonna, C., Coltelli, M. and Saltelli, A., 2008b. Sensitivity analysis and uncertainty estimation for tephra dispersal models. *Journal of Geophysical Research: Solid Earth*, 113(B6), p.B06205. [DOI]

Sparks, R.S.J., 1986. The dimensions and dynamics of volcanic eruption columns. *Bulletin of Volcanology*, 48(1), pp.3-15. [DOI]

Sparks, R.S.J., Bursik, M.I., Carey, S.N., Gilbert, J.S., Glaze, L.S., Sigurdsson, H. and Woods, A.W., 1997. *Volcanic Plumes*. John Wiley & Sons, New York, 574 pp.

Stein, A.F., Draxler, R.R., Rolph, G.D., Stunder, B.J.B., Cohen, M.D. and Ngan, F., 2015. NOAA's HYSPLIT atmospheric transport and dispersion modeling system. *Bulletin of the American Meteorological Society*, 96(12), pp.2059-2077. [DOI]

Sufitri, Y., Bachtiar, V.S., Putra, A.A. and Nugroho, S., 2024. Modeling the dispersion of air pollution due to volcanic eruptions. *International Journal of Disaster Management*, 7(3), pp.231-250. [DOI]

Suzuki, Y.J. and Koyaguchi, T., 2015. Effects of wind on entrainment efficiency in volcanic plumes. *Journal of Geophysical Research: Solid Earth*, 120(9), pp.6122-6140. [DOI]

Tadini, A., Gouhier, M., Donnadieu, F., De' Michieli Vitturi, M. and Pardini, F., 2022. Particle sedimentation in numerical modelling: A case study from the Puyehue-Cordón Caulle 2011 eruption with the PLUME-MoM/HYSPLIT models. *Atmosphere*, 13(5), p.784. [DOI]

Thivet, S., Bagheri, G., Kornatowski, P.M., Fries, A., Lemus, J., Simionato, R., Díaz-Vecino, C., Rossi, E., Yamada, T., Scollo, S. and Bonadonna, C., 2024. In-situ volcanic ash sampling and aerosol-gas analysis based on UAS technologies (AeroVolc). *Aerosol Science and Technology*, 58(5), pp.455-470. [DOI]

Torres, O., Jethva, H., Ahn, C., Jaross, G. and Loyola, D.G., 2020. TROPOMI aerosol products: evaluation and observations of synoptic-scale carbonaceous aerosol plumes during 2018–2020. *Atmospheric Measurement Techniques*, 13(12), pp.6789–6806. [DOI]

Wilson, L. and Walker, G.P.L., 1987a. Explosive volcanic eruptions - VI. Ejecta dispersal in plinian eruptions: The control of eruption conditions and atmospheric properties. *Geophysical Journal International*, 89(2), pp.657-679. [DOI]

Wilson, L. and Walker, G.P.L., 1987b. Explosive volcanic eruptions - VI. Ejecta dispersal in plinian eruptions: The control of eruption conditions and atmospheric properties. *Geophysical Journal International*, 89(2), pp.657-679. [DOI]

Woodhouse, M.J., Hogg, A.J., Phillips, J.C. and Sparks, R.S.J., 2013a. Interaction between volcanic plumes and wind during the 2010 Eyjafjallajökull eruption, Iceland. *Journal of Geophysical Research: Solid Earth*, 118(1), pp.92-109. [DOI]

Woodhouse, M.J., Hogg, A.J., Phillips, J.C. and Sparks, R.S.J., 2013b. Interaction between volcanic plumes and wind during the 2010 Eyjafjallajökull eruption, Iceland. *Journal of Geophysical Research: Solid Earth*, 118(1), pp.92-109. [DOI]

Zidikheri, M.J., Lucas, C. and Potts, R.J., 2018. Quantitative verification and calibration of volcanic ash ensemble forecasts using satellite data. *Journal of Geophysical Research: Atmospheres*, 123(8), pp.4135-4156. [DOI]